Lysosomal Membrane Permeabilization by Targeted Magnetic Nanoparticles in Alternating Magnetic Fields

Maribella Domenech,[†] Ileana Marrero-Berrios,[‡] Madeline Torres-Lugo,[†] and Carlos Rinaldi[†,§,⊥,*]

[†]Department of Chemical Engineering, University of Puerto Rico, Mayaguez, Puerto Rico 00681, United States, [‡]Industrial Biotechnology Program, University of Puerto Rico, Mayaguez, Puerto Rico 00681, United States, [§]J. Crayton Pruitt Family Department of Biomedical Engineering, University of Florida, Gainesville, Florida 32611, United States, and [⊥]Department of Chemical Engineering, University of Florida, Gainesville, Florida 32611, United States

ABSTRACT Lysosomal death pathways are being explored as alternatives of overcoming cancer tumor resistance to traditional forms of treatment. Nanotechnologies that can selectively target and induce permeabilization of lysosomal compartments in cells could become powerful medical tools. Here we demonstrate that iron oxide magnetic nanoparticles (MNPs) targeted to the epidermal growth factor receptor (EGFR) can selectively induce lysosomal membrane permeabilization (LMP) in cancer cells overexpressing the EGFR under the action of an alternating magnetic field (AMF). LMP was observed to correlate with the production of reactive oxygen species (ROS) and a decrease in tumor cell viability. Confocal microscopy images showed an increase in the cytosolic activity of the lysosomal protease cathepsin B. These observations suggest the possibility of remotely triggering lysosomal death pathways in cancer cells through the administration of MNPs which target lysosomal internalization pathways and the application of AMFs.

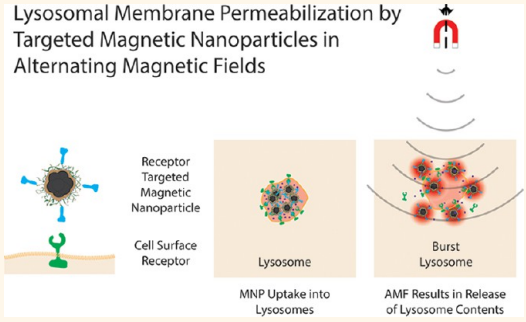

KEYWORDS: iron oxide · magnetic nanoparticles · epidermal growth factor · epidermal growth factor receptor · alternating magnetic field · lysosomal membrane permeabilization · lysosomal death pathways

Tumor resistance to undergo apoptotic cell death has become a major obstacle to successful treatment in a variety of cancers.[1,2] Poor drug circulation at the tumor site and the ability of tumor cells to evade chemotherapeutic agents results in cancer reoccurrence and development of resistance to apoptosis.[2−5] Current approaches aim to reactivate apoptotic pathways in cancer cells by employing a combination of protein-targeted agents with current anticancer drugs;[6−8] however, their success has been limited due to the ability of cancer cells to acquire more complex resistances that no longer respond to therapy.[9,10]

Recent studies have illustrated that increasing the permeability of lysosomes can be an effective strategy to promote cell death even in cancer cells with multiple defects in the classic apoptotic pathways.[11,12] Upon appropriate stimuli, the lysosome membrane becomes permeable, releasing digestive enzymes (*e.g.*, cathepsins) into the cytosol. Release of lysosomal enzymes can promote cell death through caspase dependent and caspase independent mechanisms, making it an attractive strategy to induce cancer cell death even if cells are resistant to normal apoptotic programs.[13] Additionally, lysis of lysosomes can increase the delivery of some drugs or reduce cytoplasmic pH, which may enhance the effects of some cancer treatments such as chemotherapy and hyperthermia.[14] Several strategies have been used to increase the permeability of the lysosome membrane, including use of detergents,[15] photooxidation,[16,17] lipophilic drugs,[18] and pro-apoptotic signaling.[12,19] The use of lysomotropic detergents such as siramesine has been shown to induce lysosomal leakage and cathepsin-dependent cancer cell death in mouse tumor xenografts and in *in vitro* studies.[15] Siramesine induces a rapid rise in the lysosomal pH that is followed by lysosomal leakage and dysfunction. However, siramesine induced-cytotoxicity is not

* Address correspondence to carlos.rinaldi@bme.ufl.edu.

Received for review February 11, 2013 and accepted May 21, 2013.

Published online May 21, 2013
10.1021/nn4007048

cell specific, requiring a high dose (100 mg/(kg day)) to significantly affect tumor volume in mouse xenografts.[20] Activation of LMP through chemotoxic drugs or pro-apoptotic factors has been effective in several cancer cell lines.[21,22] The cytotoxic cytokine tumor necrosis factor-α (TNF) has been shown to promote LMP through the generation of the lysosomotropic detergents ceramide and sphingosine.[22] Ceramide and sphingosine are generally toxic;[23,24] therefore, ways to deliver these components selectively to tumor cells are needed for treatment efficacy and to prevent harmful secondary side effects. Another method based on the photooxidation of thiol groups[17] in the lysosome membrane relies on the penetration of light through tissue, making it difficult to treat deep seated tumors and widespread metastatic lesions. Although these studies support the potential of LMP in killing cancer cells, they suffer from limitations such as lack of specificity, potential side effects, and inability to reach deep seated tumors. Therefore, new strategies that allow controlled and selective induction of LMP in cancer cells are of great interest to overcome multidrug resistance and increase the efficacy of current tumor therapies.

Iron oxide (IO) magnetic nanoparticles (MNPs) become associated with cells through the cell membrane or by being internalized into cellular compartments such as the lysosome. IO-MNPs exposed to an alternating magnetic field (AMF) respond by locally releasing heat and/or mechanically rotating; thus, it is possible that such response leads to disruption of phospholipid bilayers resulting in lysosomal membrane permeabilization (LMP). IO-MNPs have been shown to externally trigger controlled release of encapsulated cargo[25] where magnetic actuation was used to control timing and drug release from IO-MNP containing liposomal vesicles. During the application of an AMF, magnetic nanoparticles incorporated into a lipid bilayer vibrate and dissipate energy in the form of heat. Increased permeability of the lipid membrane was observed without increasing the bulk temperature above the melting point of the liposome (>40 °C). IO-MNPs can be rapidly concentrated in the lysosomes of tumor cells when conjugated to proteins that recognize receptors overexpressed in the cell membrane, such as the epidermal growth factor receptor (EGFR).[26] EGFR is a cell surface receptor highly overexpressed in several cancers including breast, head, neck and pancreatic cancers.[27] Upon binding of the EGF ligand to the receptor, EGFR is internalized into endosomes that later fuse with lysosomes for degradation.[28,29] Our previous work showed that internalized EGFR-targeted IO-MNPs exposed to an AMF resulted in a significant reduction (up to 99%) in tumor cell viability and clonogenic capacity without an increase in the temperature of the cell suspension.[26] This observation is significant as it demonstrates that MNPs in AMFs can kill cancer cells without a perceptible macroscopic temperature rise to the hyperthermia range of 41−47 °C, commonly believed to be required in so-called Magnetic Fluid Hyperthermia (MFH).[30,31] As the observed decrease in cell viability was thermal dose dependent and because no changes were observed in the temperature of the cell suspension, it is surmised that the reduction in cell viability is due to damage caused by the targeted MNPs to their local environment through the action of the AMF. Indeed, internalized EGFR-targeted IO-MNPs were observed mainly in the cell membrane and lysosomes, suggesting damage to these cellular components as a possible mechanism for the observed decrease in cell viability and clonogenic capacity. Thus, we speculate that IO-MNPs exposed to AMFs locally release heat and/or mechanically rotate resulting in injury to cells by denaturing proteins and permeabilizing lipid membranes. Here we evaluate the effect of EGFR-targeted IO-MNPs exposed to an AMF on the permeability of lysosomes. We hypothesized that magnetic nanoparticles conjugated to EGF would destabilize the lysosomal membrane leading to increased permeability during the application of an AMF (Figure 1). Our main goal is to use magnetic nanoparticle actuation to selectively target a wide-range of tumors independently of their apoptotic resistance mechanisms.

RESULTS

Characterization and Internalization of MNPs. Magnetic nanoparticles were synthesized by the co-precipitation method and their physical and magnetic properties were characterized (Figure 2). IO-MNPs covalently coated with carboxymethyldextran (CMDx) had a volume-weighted average hydrodynamic diameter of 61 ± 29 nm (Figure 2a) and consisted of small clusters of primary particles with diameters of 14 nm (Figure 2b). The particles possessed superparamagnetic behavior (Figure 2c). IO-MNPs (0.3 mg IO/mL) exposed to an AMF dissipated heat as a function of AMF amplitude (Figure 2c), with a SAR value of 175 ± 18 W/g at 233 kHz and 40 kA/m, corresponding to the conditions used in the experiments discussed below. The average amount of EGF per magnetic core fluctuated between 4 and 6 μg/mg, which corresponds to about 20−50 EGF molecules per 60 nm nanoparticle. We have previously demonstrated that CMDx-conjugated IO-MNPs possess colloidal stability in biological buffers and in the presence of cells.[32]

We proceeded to evaluate the amount and location of internalized IO-CMDx MNPs. Figure 3 shows representative confocal microscopy images of the distribution of MNPs (green) inside the cell. The IO-CMDx staining pattern was more diffused across the cytosol. The punctate lysosomal staining pattern (red) was very

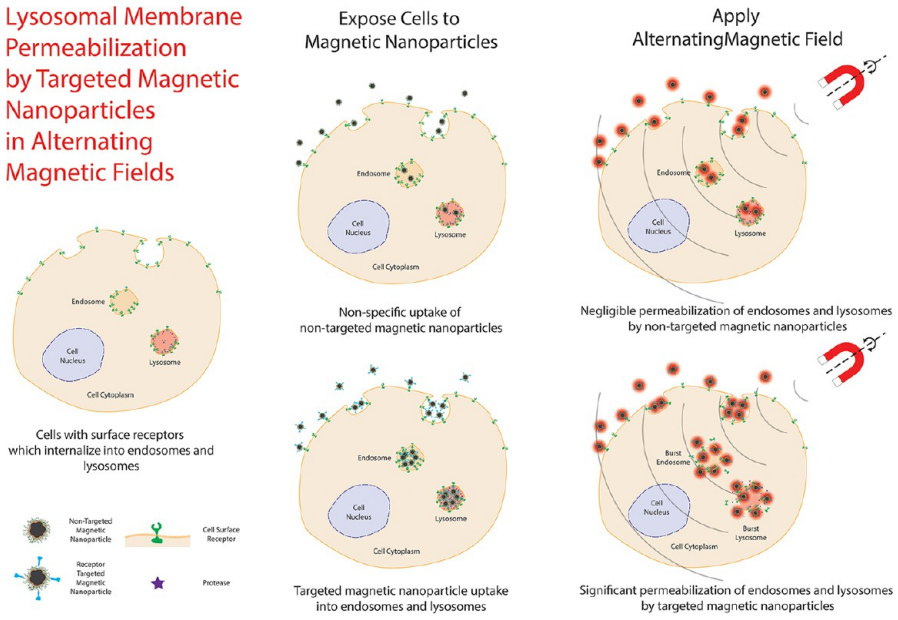

Figure 1. Schematic representation of lysosomal membrane permeabilization by magnetic nanoparticles in an alternating magnetic field. Nontargeted nanoparticles are taken up by nonspecific mechanisms, whereas targeted nanoparticles are taken up into endosomes and lysosomes due to receptor mediated endocytosis of the targeted receptor. When an alternating magnetic field is applied, both types of particles dissipate heat, with targeted magnetic nanoparticles delivering heat specifically to endosomes and lysosomes, resulting in their permeabilization and the release of their contents into the cytoplasm.

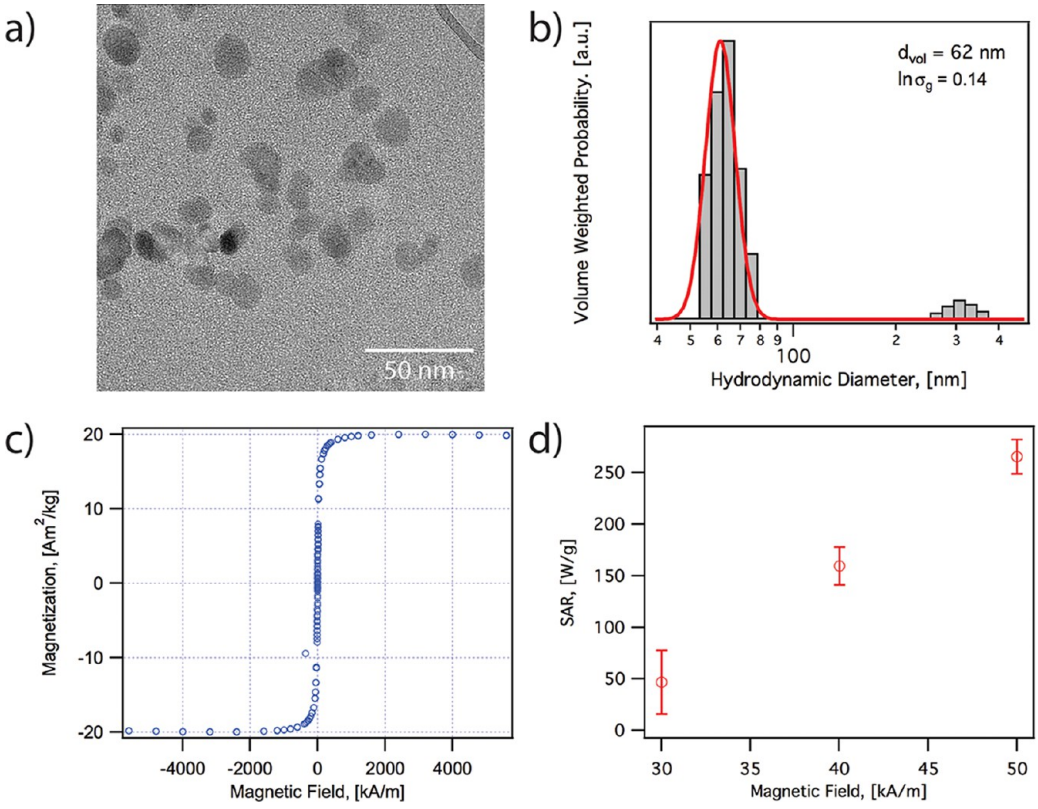

Figure 2. Characterization of iron oxide (IO) magnetic nanoparticles (MNPs). (a) Transmission electron microscopy shows particles with a mean diameter of 14 ± 4 nm. (b) Volume-weighted hydrodynamic diameter distribution for IO-CMDx MNPs in PBS 1× (0.01 mg IO/mL) with fit to log-normal distribution. (c) Equilibrium magnetization measurements of IO-CMDx MNPs at 300 K yields a magnetic diameter of 10 nm according to fit to Langevin function. (d) Specific absorption rate (SAR) measurements of IO-CMDx MNPs exposed to different magnetic field amplitudes.

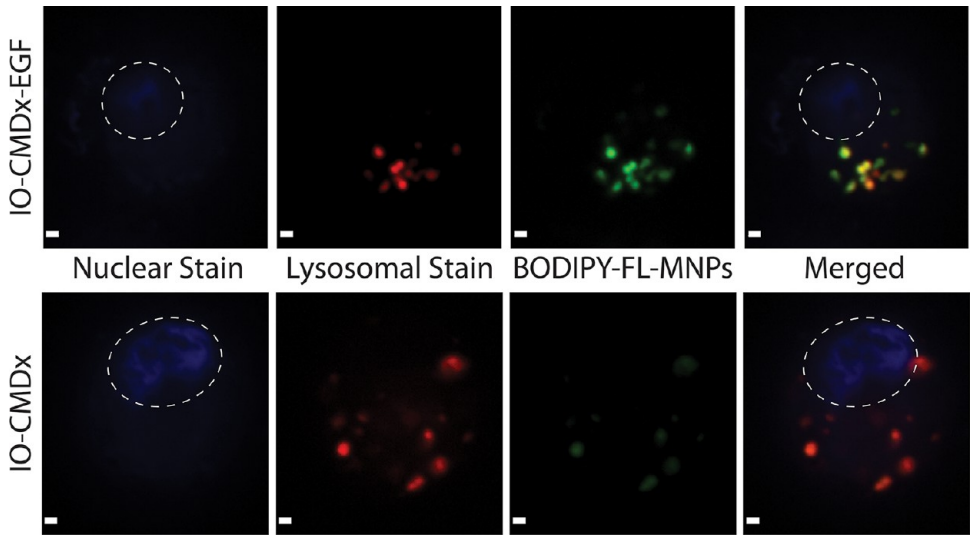

Figure 3. Intracellular distribution of MNPs in MDA-MB-231 cells. Cells were incubated with MNPs (0.3 IO mg/mL) conjugated to BODIPY-FL (green) for 2 h. Cells were visualized by fluorescence confocal microscopy at 60× magnification. Lysosomes (red) were stained with Lysotracker red (75 μM). The nucleus (blue) was stained with Hoechst 33342 (10 ug/mL). Dashed line added to outline the location of the nucleus. Scale bar represents 1 μm.

similar to the IO-CMDx-EGF staining, suggesting that IO-CMDx-EGF MNPs are concentrated inside the lysosomes. As expected, EGFR-targeted MNPs had a greater extent of internalization than nontargeted MNPs (Figure 4).

Lysosome Rupture Mediated by EGFR-Targeted MNPs in Response to an Alternating Magnetic Field. To test the hypothesis that magnetic nanoparticles conjugated to EGF can increase the permeability of the lysosome during the application of an AMF, we assayed the stability of lysosomes in cells loaded with MNPs and exposed to an AMF. The AMF oscillated at a frequency of 233 kHz and had a magnitude of 42 kA/m. The acridine orange (AO) uptake-method was used to determine lysosomal rupture.[33,34] AO is a lysomotropic dye permeable to the cell membrane that fluoresces red inside the lysosomes and weakly green when bound to DNA or in the cytosol. Ruptured lysosomes do not contribute to AO uptake resulting in a population of cells with reduced red fluorescence (pale cells). Cells treated with hydrogen peroxide (H_2O_2), an inducer of oxidative stress, were used as a positive control of lysosomal membrane damage. As shown in Figure 5, cells treated with targeted MNPs and exposed to an AMF show a significant increase in the number of pale cells, as compared to control (0 kHz) and EGF (233 kHz) groups. Although nontargeted MNPs are more widespread inside the cell as compared to targeted-MNPs, a small increase in the number of pale cells was observed in cells treated with nontargeted MNPs (IO-CMDx) and exposed to an AMF. This increase in lysosome permeability could be caused by heat dissipation or rotation by MNPs adjacent to lysosomes or internalized into lysosomes through nonspecific cellular uptake pathways.

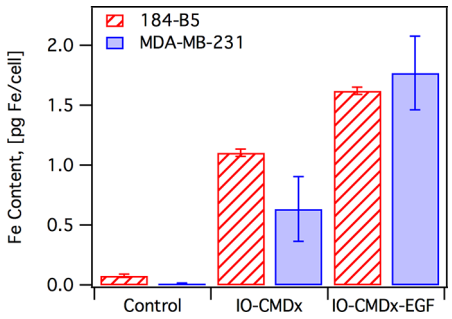

Figure 4. Cellular uptake of targeted and nontargeted magnetic nanoparticles in MDA-MB-231 cancer cells. Attached cells were incubated with MNPs (IO 0.3 mg/mL) for 2 h. Cell samples were washed three times to remove unbound MNPs and digested in nitric acid. IO-CMDx-EGF MNPs had higher uptake than IO-CMDx. Bars show the average iron content per cell. Data represent the mean of 3 independent experiments ± SE.

Cathepsins are proteolytic enzymes located in the lysosomal compartment. The release of cathepsins into the cytosol can result as a consequence of lysosomal rupture. To further confirm lysosomal rupture in response to an AMF, we monitored the cytosolic activity of cathepsin B using Magic Red (RR)2. Peptide (RR)2 is a cathepsin B specific substrate permeable to the cell membrane. Cleavage of (RR)2 by cathepsin B releases a fluorescent form of the cresyl violet fluorophore. Confocal microscopy images (Figure 6a) show that cells treated with MNPs and exposed to an AMF contain lysosomes with very little cathepsin B activity (white arrows). Confocal imaging analysis of 3D image stacks of single cells shows that cytosolic activity of cathepsin B (outside the lysosomes) was higher in cells treated with EGFR-targeted IO-MNPs and exposed to an AMF (Figure 6b).

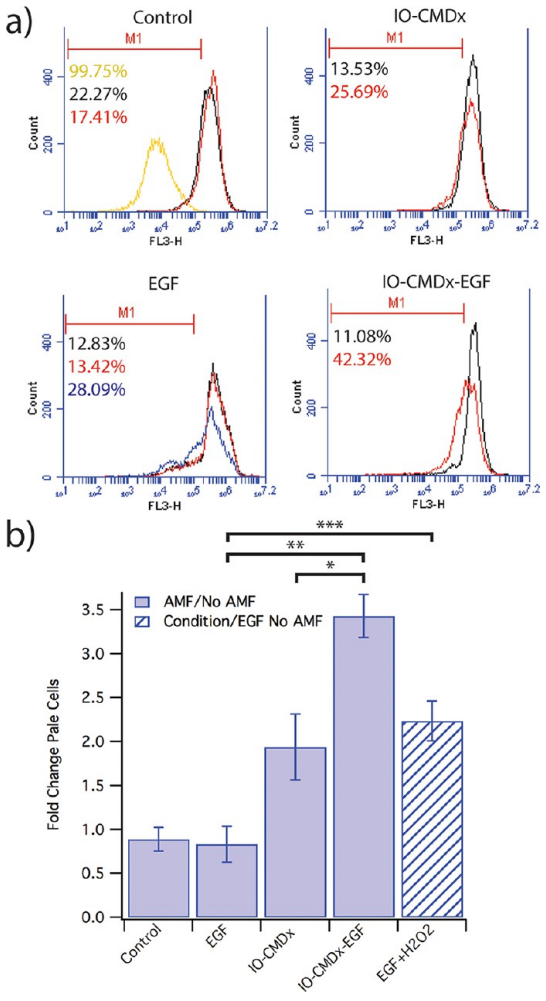

Figure 5. Magnetic nanoparticles exposed to an alternating magnetic field induce lysosomal membrane permeabilization. (a) MDA-MB-231 cells were treated with MNPs and exposed to an alternating magnetic field (AMF, 233 kHz, 41.75 kA/m, red peak) or left in the incubator (No AMF, black peak) for 1 h. Lysosomes were stained with AO (10 μg/mL) for 10 min and the % of pale cells was quantified by flow cytometry in FL-3 channel. M1 represents the region of pale cells and it was determined by placing the marks around the peak enclosing unstained cells (no acridine orange, yellow peak). Hydrogen peroxide (H_2O_2) was used as a positive control for LMP (blue peak). Peak diagrams are representative of one independent experiment. (b) Bars show the fold increase in the number of pale cells exposed to the AMF normalized to the same condition without field (No AMF) EGF-H_2O_2 condition was normalized to EGF without field (EGF No AMF). Data represent the mean of 4 independent experiments ± SE. *$p < 0.1$, **$p < 0.01$, ***$p < 0.005$.

Cell Toxicity. Permeabilization of the lysosome membrane has been shown to promote cell death.[35,36] The release of proteolytic enzymes into the cytosol can directly promote or participate in apoptotic signaling. To determine the impact of LMP mediated by magnetic actuation of EGFR-targeted MNPs on cell death, we evaluated cell viability in MDA-MB-231 and 184-B5 cells 48 h post-treatment. MDA-MB-231 cells treated with EGFR-targeted MNPs and exposed to an AMF show a significant decrease in cell viability as compared to nontargeted MNPs and EGF treatment (Figure 7). Nontargeted MNPs did not affect cell viability suggesting that the extent and location of nanoparticles taken up by the cell is an important determinant in MNP-mediated cell death. Although increased LMP was observed in 184-B5 cells treated with IO-CMDx-EGF and exposed to an AMF (Figure 8), cellular viability was not affected by exposure to an AMF (Figure 7). Normal cells divide more slowly and have less protein mutations compared to tumor cells which may allow them to recover from heat/mechanical damage caused by MNPs to proteins and lipid membranes.[37,38]

Increased production of reactive oxygen species (ROS) can lead to uncontrolled lysosomal permeability *via* massive peroxidation of membrane lipids. The generation of ROS can occur inside or outside the lysosomal compartment. During the application of an AMF, ROS can be released from the mitochondria as a response to thermal damage induced by heat dissipation from magnetic nanoparticles inside the cells. We evaluated the production of ROS using a nonfluorescent cell-permeable dye that reacts directly with a wide range of reactive species such as hydrogen peroxide, peroxynitrite and hydroxyl radicals, yielding a green fluorescent product indicative of cellular production of ROS. Cells treated with targeted MNPs show an increase in ROS when exposed to an AMF (Figure 9a), whereas no significant change was observed with nontargeted MNPs exposed to an AMF. In the absence of an AMF, exposure of cells to EGF alone and to targeted/nontargeted MNPs did not result in a significant change in ROS relative to the control of cells in the incubator. These observations indicate that ROS production in the cells exposed to targeted MNPs and an AMF is associated to damage caused to cellular components due to heat dissipated or mechanical disruption generated by the targeted MNPs.

DISCUSSION

Because MNPs in AMFs respond by locally releasing heat and/or mechanically rotating, it is possible that such response leads to disruption of phospholipid bilayers resulting in permeabilization of the lysosomal membrane. Indeed, molecular simulations of rupture in lipid bilayers demonstrate that both incremental tension and incremental shear can destabilize cell membranes[39] and that the energy required to achieve such membrane rupture is achievable with rotating MNPs in AMFs. Alternatively, energy dissipated locally as heat by MNPs in AMFs could lead to disruption of lipid membranes. Huang *et al.*[40] demonstrated a temperature-induced change in fluorescence of a fluorophore attached to MNPs exposed to AMFs, whereas a free fluorophore underwent no change. They claimed

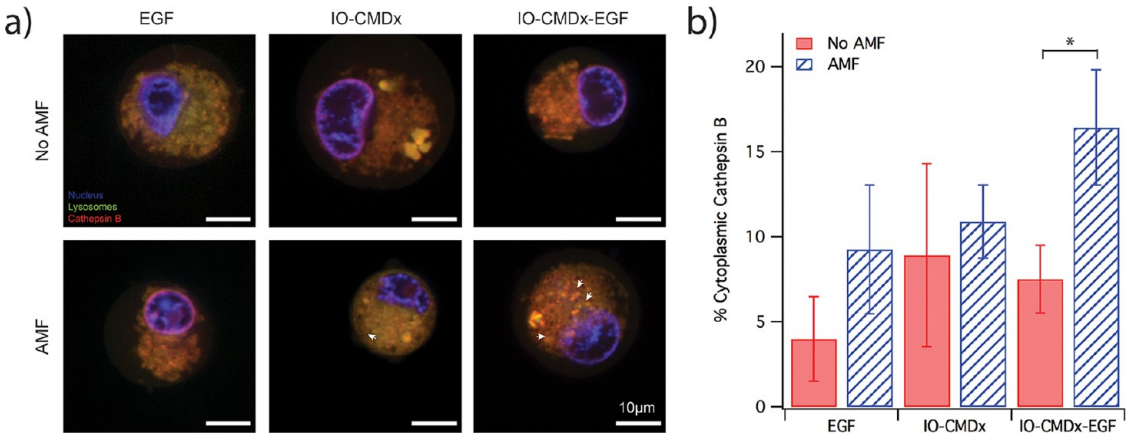

Figure 6. Cathepsin B release in response to an alternating magnetic field. MDA-MB-231 cells were treated with IO-MNPs and exposed to an alternating magnetic field (233 kHz, 41.75 kA/m, AMF) or left in the incubator (No AMF) for 1 h. (a) Lysosomes were stained in green with lysotracker green (1 μM), nucleus in blue with Hoecsht (10 μg/mL) and cathepsin B activity in red using Magic Red (RR)2. Confocal images of suspended cells were obtained with a 60× objective. White arrows point to lysosome vesicles with low cathepsin B activity. (b) Five single cell images were randomly obtained and analyzed per condition. SlideBook 5.0 software was used to determine cathepsin B subcellular location from 3D-image stacks. Data represents the mean ± 1SD. *$p < 0.1$.

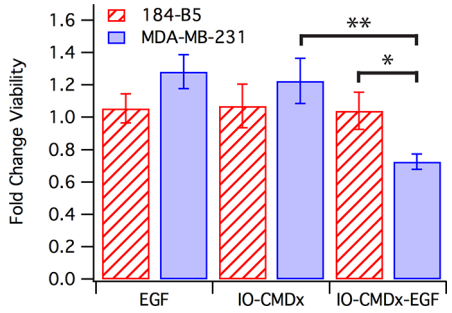

Figure 7. Cell viability. MDA-MB-231 and 184-B5 cells were incubated with IO-MNPs and exposed to an alternating magnetic field (AMF, 233kHz, 41.75 kA/m). Magnetic field controls were left in the incubator (No AMF) for 1 h. A total of 10 000 cells were seeded in 96 well plates and cell viability was evaluated 48 h post-treatment. Data represent the mean fold change in viability relative to the incubator control of 4 independent experiments ± 1 SE. *$p < 0.1$, **$p < 0.05$.

that a local increase of the nanoparticle surface temperature was responsible for the observed increase in fluorescence.[40] Experimentally, we have shown that a thermoresponsive polymer attached to IO-MNPs undergoes its transition when exposed to an AMF even while the bulk temperature is below the transition temperature.[41] These two studies demonstrate that energy dissipated locally by MNPs in AMFs can lead to changes in molecules in close proximity to the nanoparticle surface. Furthermore, Amstad *et al.*[25] showed that magnetic actuation could be used to control timing and drug release from vesicles containing iron oxide nanoparticles. Upon the application of an AMF, iron oxide containing liposomes released their cargo, even though the heat released was insufficient to heat bulk water to the membrane melting temperature. This suggests that energy dissipated by MNPs associated to lipid membranes in AMFs can lead to their permeabilization. In a biological context, EGFR-targeted magnetic nanoparticles in AMFs were shown to significantly reduce viability and proliferation of cancer cells without a perceptible macroscopic temperature rise[26] and in a heat dose dependent manner. These observations were attributed to damage to proteins, cellular compartments, or the cell membrane caused by the rotation and/or heat dissipation due to the targeted MNPs in AMFs, however, these mechanisms were not tested.

Nanoparticles become associated with cells through the cell membrane or by being internalized into cellular compartments such as endosomes and lysosomes. We took advantage of the endocytic trafficking of the EGFR to evaluate the effect of EGF-coated MNPs in LMP. Our results show that EGFR-targeted IO-MNPs increase the permeability of the lysosome membrane when exposed to an AMF. The increase in LMP correlated with a decrease in cancer cell viability and an increase in ROS in cells treated with EGFR-targeted MNPs and AMFs. Although we believe that LMP is involved in the observed cancer cell toxicity, other mechanisms such as proteotoxic stress and pro-apoptotic signaling might play an important role in MNP-induced tumor cell toxicity. Identifying the key mechanisms involved in MNP-mediated tumor cell death will be part of our future studies.

EGFR is highly overexpressed in many cancers and its activation can promote processes responsible for tumor growth and progression. Targeting MNPs to the EGFR can increase the selectivity of MNPs toward cancer cells. Importantly, our results show that viability of normal cells was not significantly affected by EGFR-targeted MNPs or LMP. This suggests that manipulation of LMP with EGFR-targeted MNPs can be used to

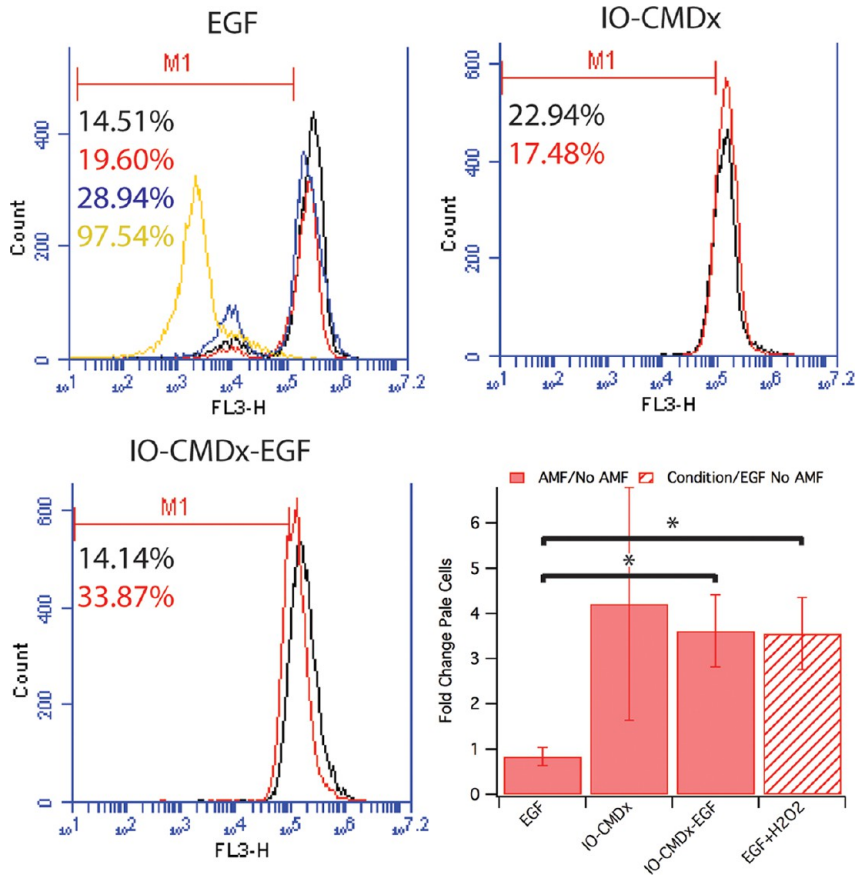

Figure 8. Magnetic nanoparticles exposed to an alternating magnetic field induce lysosomal membrane permeabilization (LMP) in 184-B5. Cells were treated with MNPs and exposed to an alternating magnetic field (AMF, 233 kHz, 41.75 kA/m, red peak) or left in the incubator (No AMF, black peak) for 1 h. Lysosomes were stained with acridine orange (10ug/mL) for 10 min and the percentage (%) of pale cells was quantified by flow cytometry in the FL-3 channel. M1 represents the region of pale cells and it was determined by placing the marks around the peak enclosing unstained cells (no acridine orange, yellow peak). Hydrogen peroxide (H_2O_2) was used as a positive control for LMP (blue peak). Exogenous addition of EGF is required to maintain 184-B5 growing in culture; therefore, EGF was used as a normal culture control. Peak diagrams are representative of one independent experiment. Bars show the fold-increase in the number of pale cells exposed to the AMF normalized to the same condition with no field (No AMF). EGF-H_2O_2 condition was normalized to EGF No AMF. Data represent the mean of 3 independent experiments ± SE. *$p < 0.1$.

selectively promote cancer cell death while minimizing damage to normal tissues. In previous studies, we have shown that reductions in cancer cell viability of up to 99% are possible depending on the heat dose, amount of internalized MNPs and apoptotic EGFR signaling.[26] The amount of MNPs internalized in cells can be increased by locally applying a steady magnetic field gradient, which has been shown to substantially increase cellular uptake *in vitro*[42] and served to enrich MNP concentration at the tumor site *in vivo*.[43,44] To minimize the variability in cytotoxicity associated to the signaling mechanism (proliferative or apoptotic) triggered by EGF-conjugated MNPs bound to EGFR, other EGFR targets that inhibit receptor signaling while retaining endocytosis, such as EGFR antibody Cetuximab,[45] should be evaluated.

Increased permeability of the lysosome membrane not only can be used to promote cancer cell death through the release of proteolytic enzymes and increase in ROS, but can also enhance the efficacy of drugs trapped in lysosomes. Lysosomal drug sequestration plays an important role in the development of tumor drug resistance.[18] Lysosomotropic drugs, such as amine and weak basic compounds, become protonated inside the acidic lysosome and are unable to escape into the cytosol. Although lysosomes are small, they can accumulate many drugs at up to 100-fold higher concentration than the extracellular environment.[46,47] Consequently, lysosomal drug trapping is responsible for 25−40% of whole tissue drug uptake.[48] MNP-mediated LMP could be used to treat multidrug resistance by altering the subcellular distribution of drugs in combination with heat-generated proteolytic damage and proteotoxic stress. MNP-mediated LMP can be used in combination with conventional clinical treatments (*e.g.*, chemotherapy, radiation), anti-cancer agents such as proteins can be conjugated to the MNPs,[49] and whole body magnetic field applicators[50] can be used to deliver the required

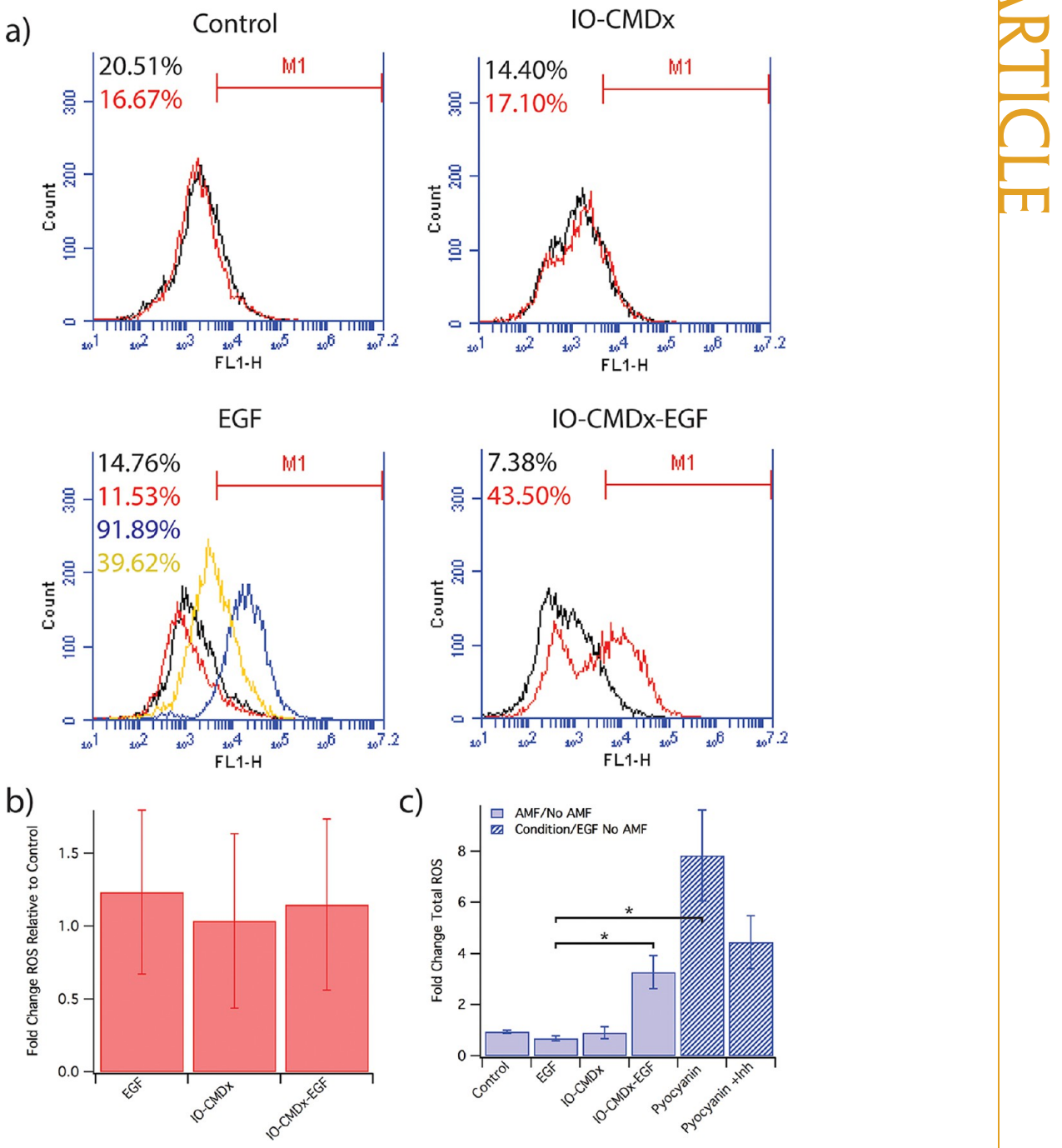

Figure 9. Generation of reactive oxygen species (ROS) in response to an alternating magnetic field. (a) MDA-MB-231 cells were treated with MNPs and exposed to an alternating magnetic field (AMF, 233kHz, 41.75 kA/m, red peak) or left in the incubator (No AMF, black peak) for 1 h. Intracellular ROS was detected using flow cytometry in the FL-1 channel. M1 represents the region below which there is normal ROS expression. Pyocyanin (blue peak) and pyocyanin + inhibitor (yellow peak) were used as positive controls for ROS formation. Peak diagrams are representative of one independent experiment. (b) Bars show the fold increase in the number of MDA-MB-231 cells with ROS normalized to control when exposed to various conditions in the absence of an AMF. (c) Bars show the fold increase in the number of MDA-MB-231 cells with ROS when exposed to AMF. Mean values were normalized to the same condition with No AMF. Pyocyanin and pyocyanin + inhibitor conditions were normalized to EGF No AMF. Data represent the mean of 4 independent experiments ± SE. *$p < 0.05$.

magnetic fields anywhere in the body, including deep tissues.

CONCLUSIONS

The development of cancer treatments with different modes of action is of key importance in overcoming cancer cell resistance to therapy. Due to the ability of LMP to promote cell death independently of apoptosis resistance mechanisms, the activation of lysosomal death pathways has been suggested as a potential cancer treatment. Unfortunately, drugs that trigger this pathway face serious

limitations. We have shown that MNPs targeted to the lysosome and exposed to AMF are a novel strategy to manipulate LMP, selectively killing the targeted cancer cells.

MATERIALS AND METHODS

Synthesis and Characterization of MNPs. Iron oxide magnetic nanoparticles (IO-MNPS) were synthetized by the co-precipitation of two iron salts, as described by Creixell *et al.*[26] IO-MNPs were peptized with $(CH_3)_4NOH$ and functionalized with an aminosilane (APS) to graft functional amine groups in MNPs (IO-APS). Formation of amide bonds with carboxylmethyl dextran (CMDx) was achieved *via* EDC/NHS reaction. Briefly, 25 mg of EDC (22980, ThermoScientific, Rockford, IL), 15 mg of NHS (130672, Sigma-Aldrich, St. Louis, MO) and 1 g of CMDx (86524, Sigma-Aldrich) dissolved in 10 mL of deionized water (pH 4.5−5) were mixed with 0.1 g of IO-APS. Unbound CMDx was removed by a series of washes with ethanol/water mixture (3:1) and centrifugation steps (8000 rpm for 10 min) until no more CMDx (light brown-yellow color) was observed in the organic phase (3−4 washes). IO-CMDx MNPs were dried at 60 °C in a vacuum oven and stored at 4 °C. MNPs functionalized with CMDx were washed three times with ethanol, dried at 60 °C in a vacuum oven and stored at 4 °C. For biological experiments, MNPs were autoclaved and suspended in cell culture media or PBS 1× by ultrasonication for 5−10 min. CMDx-conjugated MNPs suspended in PBS 1× (0.01 mg IO/mL) have a hydrodynamic diameter of approximately 60 nm (Brookhaven Instruments BI-90 Plus Particle Size Analyzer). The weight percentage of magnetic core was estimated from thermo-gravimetric analysis (TA Instruments 2950). The magnetic properties of the nanoparticles were evaluated using a magnetometer (Quantum Design MPMS XL-7 SQUID). For specific absorption rate (SAR) measurements, 0.3 mg of magnetic core diluted in 1 mL of PBS 1× were exposed to increasing magnetic field intensity for 100 s. Sample temperature was monitored with a Luxotron Fluoroptic Thermoprobe.

Conjugation of EGF to MNPs. Sterilized MNPs (6 mg magnetic core) were suspended in 2.5 mL of PBS 1× and mixed with 0.5 mL of 120 mg/mL EDC (sterilized by filtration) for 10 min (pH 4.5−5) at room temperature (25 °C). The solution was adjusted to pH 7.8 and 200 μg of EGF (Z00333, GenScript, Piscataway, NJ) was added to the particle solution. The solution was incubated for 2−4 h at 37 °C in a thermoshaker at 200 rpm. Unbound EGF was removed by 3 rounds of washes with PBS 1× dialyzed using 30K centrifugal tubes centrifuged at 7000 rcf for 10 min at 4 °C as previously determined by Creixell *et al.*[51] EGF concentration on the surface of magnetic nanoparticles was quantified using the CBQCA Protein Quantitation kit (C6667, Invitrogen, Eugene, OR). The CBQCA assay quantifies proteins by binding of 3-(4-carboxybenzoyl) quinolone-2-carboxaldelhyde (CBQCA) to amines in the presence of thiols or cyanide at basic pH 9. The fluorescent product of CBQCA has an absorption peak excitable at 430−490 nm with maximum emission at around 560 nm. The amount of EGF in magnetic nanoparticles was estimated in nanoparticles that had the free amine groups of APS blocked with glutaraldehyde down to undetectable levels prior to EGF conjugation. Briefly, 12 mg of magnetic core was suspended in 2 mL of 10 mM sodium phosphate buffer and mixed with 2 mL of 20% glutraldehyde solution. The mixture was incubated at 200 rpm for 1 h at room temperature. Unbound glutaraldehyde was removed by 3 rounds of washes with PBS 1× dialyzed using 30K centrifugal tubes (Millipore) centrifuged at 7000 rcf for 10 min at 4 °C. To obtain accurate estimates of the amount of EGF on the surface of MNPs, EGF was conjugated to IO-CMDx-G and IO-CMDx in parallel reactions.

Cell Culture. The human breast cell lines MDA-MB-231 (cancer derived) and 184-B5 (normal tissue) were purchased from American Type Culture Collection (Rockville, MD). Cells were cultured in 25 cm^2 cell culture flasks (Costar Corning, Lowell, MA) and maintained at 37 °C and 5% CO_2. MDA-MB-231 were cultured in DMEM (56499C, Sigma-Aldrich) containing 4500 mg/L dextrose, 4.0 mM L-glutamine, 110 mg/L sodium pyruvate, 10% fetal bovine serum (10082, Invitrogen), 0.1 mM nonessential amino acids (11140, Invitrogen), 1 μg/mL streptomycin (15140, Invitrogen), 1 units/mL penicillin (15140, Invitrogen), 2.5 μg/mL amphotericin B (A-2942, Sigma-Aldrich) and 2.7 g/L of sodium bicarbonate (s8875, Sigma-Aldrich). 184-B5 cells were cultured in MEGM supplemented with gentamyocin, EGF, insulin and 2% bovine pituitary extract (CC-3150, Lonza, Walkersville, MD). Cells were used within passages 10−25.

Internalization and Localization of MNPs. BODIPY-FL (D2184, Invitrogen) was bound to the free amine groups of APS in IO-CMDx *via* EDC/NHS reaction as previously described. About 200 000 cells were seeded in 2-well chamber slides (155380, Thermo Scientific) and treated with 0.3 mg of FeO/mL for 2 h. Lysotracker red −DND99 (L7528, Invitrogen) and Hoescht 33342 (H3570, Invitrogen) were added at a final concentration of 0.75 μM and 10 μg/mL, respectively, during the last 30 min of incubation. Cell samples were washed twice with PBS 1× to remove free dyes and MNPs prior to imaging. To measure iron content inside cells, pelleted cells were resuspended in 200 μL of ultrapure water to obtain a homogeneous cell suspension. The suspended cells were transferred into glass tubes containing 70% HNO_3 and then mineralized until completely dried at 80 °C. The mineralized sample was dissolved in 4 mL of 2% HNO_3 in ultrapure water. ICP measurements obtained from samples were compared to iron standard (Fe^{3+}) to determine iron concentration.

AMF Treatment. Attached cells seeded overnight at a density of 225 000 MDA-MB-231 cells/well (6 well plates) were incubated with cell culture media (DMEM 10% FBS) containing EGF 2−5 μg/mL (equivalent [EGF] as in 0.3 mg core/mL of IO-CMDx-EGF), IO-CMDx or IO-CMDx-EGF (0.3 mg FeO/mL) for 2 h at 37 °C and 5% CO_2. Unbound MNPs were removed by 3 consecutive washes with 2 mL of PBS 1× per culture well. Cells were detached (tripsin 0.5%) and suspended in 2 mL of cell culture media. A commercial induction heater setup (RDO Induction, Washington, NJ) with an operating frequency of 233kHz and magnetic field intensities of 0−62.8 kA/m was used as the magnetic field source. A 4-loop round copper coil of 2 cm inner diameter was connected to the RDO Induction heater to generate an AMF in the sample. Two milliliters of cell suspension (110 000 cells) contained in a 5 mL glass vial was placed inside the coil. A layer of foam (0.4 cm) was placed around the glass vial to tightly hold the tube in place and to thermally isolate the sample from the induction heater coils. The distance between the coil and the glass vial was the same as the thickness of the foam layer. Cold water (16 °C) recirculated inside the induction coil also to protect the sample from heat dissipated by the oscillating electric current in the coil. An external heating box was used to maintain the environmental temperature at 37 °C ± 0.3 °C. Cell suspensions were exposed to an AMF (42 kA/m, 233 kHz) or left in the incubator (37 °C) for 1 h. The temperature of the sample and environment were measured using fluoroptic immersion probes connected to a Luxtron Fluoroptic Thermometry Lab module (Lumasense Technologies, Oakland, NJ).

Lysosome Membrane Stability Assays. Lysosome membrane stability was evaluated in single cells using AO-uptake method. AO is a metachromatic fluorophore and a lysomotropic base that becomes protonated within acidic compartments mainly mature lysosomes (pH 4.5−5). Lysosomes loaded with AO emit an intense red fluorescence (FL-3 channel) when excited by blue light (488 nm argon laser). A total of 50−80 000 cells suspended in 500 μL of cell culture media were treated with Acridine Orange (10 μg/mL) for 10 min at 37 °C. Treatment with 0.3 μM hydrogen peroxide (H_2O_2) for 30−45 min was used as a positive control for lysosome permeability. Nonstained cells were used to determine the region of pale cells (M1 region). Single cells with a reduced number of AO loaded lysosomes (pale cells) were measured with a benchtop Accuri C6 flow cytometer

(BD Biosciences, Franklin Lakes, NJ). CFlow Plus software (BD Biosciences) was used for acquisition and analyses.

Cathepsin B Activity. Following AMF treatment, cathepsin B activity was evaluated *in situ* using the Magic Red TM Cathepsin B Detection kit (937, Immunochemistry Technologies, LLC, Bloomington, MN). Lysosomes and the nucleus were stained with Lysotracker Green DND-26 (L-7526, Invitrogen) and Hoescht 33342, respectively. About 20 μL of cell suspension was placed between 2 coverslips to obtain confocal 3D image stacks of single cells.

Intracellular ROS. Intracellular ROS was detected using the Total ROS Detection Kit (ENZ-51011, Enzo Life Sciences Inc., Farmindale, NY) following the manufacturer's recommended protocol. Following AMF treatment, approximately 90 000 cells suspended in cell culture media were treated with ROS Detection Solution for 30 min at 37 °C in the dark. Cells treated with Pyocyanin (500 μM) $\pm$ 5 mM ROS Inhibitor (*N*-acetyl-L-cysteine) for 30 min were used as a positive control for ROS generation. Upon staining, cell fluorescence was collected in the FL-1 channel (488 nm) of the AccuriC6 flow cytometer. CFlow Plus software was used for acquisition and analyses.

Cell Viability. Following AMF treatment, about 7−10 000 cells/well (96 well plates) were seeded in 200 μL of cell culture media for 48 h. Cells were washed once with PBS 1$\times$ (100 μL/well). Cellular toxicity was evaluated immediately with CellTiter Blue (Promega, Madison, WI) following manufacturer's recommendation.

Image Analysis and Statistics. Images of live cells were obtained using a confocal spinning disk microscope (3i Systems Olympus IX81, Denver, CO) with a 60$\times$ oil objective (NA:1.42, RI:0.17) and a QImaging camera (SN:Q31153). For co-localization analysis, masks for each dye were generated applying the Ridler-Calvard method. Percentage of co-localization was generated for each 3D image stack and compared among conditions. The Slidebook 5.0 software was used for image acquisition and co-localization analysis.

Data represents the mean $\pm$ standard error (SE) of at three to four independent experiments as specified. For comparisons of two means, Student's *t* test was used. Significant changes were determined based on *p*-values: $p < 0.05$ (*) and $p < 0.005$ (**).

Conflict of Interest: The authors declare no competing financial interest.

Acknowledgment. The authors are grateful to Dr. Francois Orange (Department of Physics at University of Puerto Rico, San Juan, PR) for the acquisition and analysis of images obtained in TEM. This work was supported by the US National Science Foundation, through grants CBET-0609117, HRD-0833112, and EPS-1002410.

REFERENCES AND NOTES

1. Gillet, J. P.; Gottesman, M. M. Mechanisms Of Multidrug Resistance in Cancer. *Methods Mol. Biol.* **2010**, *596*, 47–76.
2. Gottesman, M. M. Mechanisms of Cancer Drug Resistance. *Annu. Rev. Med.* **2002**, *53*, 615–627.
3. Calcagno, A. M.; Salcido, C. D.; Gillet, J. P.; Wu, C. P.; Fostel, J. M.; Mumau, M. D.; Gottesman, M. M.; Varticovski, L.; Ambudkar, S. V. Prolonged Drug Selection of Breast Cancer Cells and Enrichment of Cancer Stem Cell Characteristics. *J. Natl. Cancer Inst.* **2010**, *102*, 1637–1652.
4. Gottesman, M. M.; Fojo, T.; Bates, S. E. Multidrug Resistance in Cancer: Role of ATP-Dependent Transporters. *Nat. Rev. Cancer* **2002**, *2*, 48–58.
5. Tolomeo, M.; Simoni, D. Drug Resistance and Apoptosis in Cancer Treatment: Development of New Apoptosis-Inducing Agents Active in Drug Resistant Malignancies. *Curr. Med .Chem. Anticancer Agents* **2002**, *2*, 387–401.
6. Maione, P.; Gridelli, C.; Troiani, T.; Ciardiello, F. Combining Targeted Therapies and Drugs with Multiple Targets in the Treatment of NSCLC. *Oncologist* **2006**, *11*, 274–284.
7. Rodriguez-Enriquez, S.; Marin-Hernandez, A.; Gallardo-Perez, J. C.; Carreno-Fuentes, L.; Moreno-Sanchez, R. Targeting of Cancer Energy Metabolism. *Mol. Nutr. Food Res.* **2009**, *53*, 29–48.
8. Diaz, A.; Leon, K. Therapeutic Approaches to Target Cancer Stem Cells. *Cancers* **2011**, *3*, 3331–3352.
9. Bao, S.; Wu, Q.; McLendon, R. E.; Hao, Y.; Shi, Q.; Hjelmeland, A. B.; Dewhirst, M. W.; Bigner, D. D.; Rich, J. N. Glioma Stem Cells Promote Radioresistance by Preferential Activation of the DNA Damage Response. *Nature* **2006**, *444*, 756–760.
10. Ishikawa, F.; Yoshida, S.; Saito, Y.; Hijikata, A.; Kitamura, H.; Tanaka, S.; Nakamura, R.; Tanaka, T.; Tomiyama, H.; Saito, N.; *et al.* Chemotherapy-Resistant Human AML Stem Cells Home to and Engraft within the Bone-Marrow Endosteal Region. *Nat. Biotechnol.* **2007**, *25*, 1315–1321.
11. Kirkegaard, T.; Jaattela, M. Lysosomal Involvement in Cell Death and Cancer. *Biochim. Biophys. Acta* **2009**, *1793*, 746–754.
12. Erdal, H.; Berndtsson, M.; Castro, J.; Brunk, U.; Shoshan, M. C.; Linder, S. Induction of Lysosomal Membrane Permeabilization by Compounds That Activate P53-Independent Apoptosis. *Proc. Natl. Acad. Sci. U.S.A.* **2005**, *102*, 192–197.
13. Jaattela, M. Multiple Cell Death Pathways as Regulators of Tumour Initiation and Progression. *Oncogene* **2004**, *23*, 2746–2756.
14. Lin, C. W.; Shulok, J. R.; Kirley, S. D.; Bachelder, C. M.; Flotte, T. J.; Sherwood, M. E.; Cincotta, L.; Foley, J. W. Photodynamic Destruction of Lysosomes Mediated by Nile Blue Photosensitizers. *Photochem. Photobiol.* **1993**, *58*, 81–91.
15. Ostenfeld, M. S.; Hoyer-Hansen, M.; Bastholm, L.; Fehrenbacher, N.; Olsen, O. D.; Groth-Pedersen, L.; Puustinen, P.; Kirkegaard-Sorensen, T.; Nylandsted, J.; Farkas, T.; *et al.* Anti-Cancer Agent Siramesine Is a Lysosomotropic Detergent That Induces Cytoprotective Autophagosome Accumulation. *Autophagy* **2008**, *4*, 487–499.
16. Wan, F. Y.; Wang, Y. N.; Zhang, G. J. Influence of the Physical States of Membrane Surface Area and Center Area on Lysosomal Proton Permeability. *Arch. Biochem. Biophys.* **2002**, *404*, 285–292.
17. Wan, F. Y.; Zhang, G. J. Enhancement of Lysosomal Proton Permeability Induced by Photooxidation of Membrane Thiol Groups. *Arch. Biochem. Biophys.* **2002**, *402*, 268–274.
18. Kornhuber, J.; Henkel, A. W.; Groemer, T. W.; Stadtler, S.; Welzel, O.; Tripal, P.; Rotter, A.; Bleich, S.; Trapp, S. Lipophilic Cationic Drugs Increase the Permeability of Lysosomal Membranes in a Cell Culture System. *J. Cell Physiol.* **2010**, *224*, 152–164.
19. Foghsgaard, L.; Wissing, D.; Mauch, D.; Lademann, U.; Bastholm, L.; Boes, M.; Elling, F.; Leist, M.; Jaattela, M. Cathepsin B Acts as a Dominant Execution Protease in Tumor Cell Apoptosis Induced by Tumor Necrosis Factor. *J. Cell Biol.* **2001**, *153*, 999–1010.
20. Ostenfeld, M. S.; Fehrenbacher, N.; Hoyer-Hansen, M.; Thomsen, C.; Farkas, T.; Jaattela, M. Effective Tumor Cell Death by Sigma-2 Receptor Ligand Siramesine Involves Lysosomal Leakage and Oxidative Stress. *Cancer Res.* **2005**, *65*, 8975–8983.
21. Xiang, J.; Chao, D. T.; Korsmeyer, S. J. BAX-Induced Cell Death May Not Require Interleukin 1 Beta-Converting Enzyme-Like Proteases. *Proc. Natl. Acad. Sci. U.S.A.* **1996**, *93*, 14559–14563.
22. Ullio, C.; Casas, J.; Brunk, U. T.; Sala, G.; Fabrias, G.; Ghidoni, R.; Bonelli, G.; Baccino, F. M.; Autelli, R. Sphingosine Mediates TNFα-Induced Lysosomal Membrane Permeabilization and Ensuing Programmed Cell Death in Hepatoma Cells. *J. Lipid Res.* **2012**, *53*, 1134–1143.
23. Taha, T. A.; Mullen, T. D.; Obeid, L. M. A House Divided: Ceramide, Sphingosine, and Sphingosine-1-Phosphate in Programmed Cell Death. *Biochim. Biophys. Acta* **2006**, *1758*, 2027–2036.
24. Suzuki, E.; Handa, K.; Toledo, M. S.; Hakomori, S. Sphingosine-Dependent Apoptosis: A Unified Concept Based on Multiple Mechanisms Operating in Concert. *Proc. Natl. Acad. Sci. U.S.A.* **2004**, *101*, 14788–14793.
25. Amstad, E.; Kohlbrecher, J.; Muller, E.; Schweizer, T.; Textor, M.; Reimhult, E. Triggered Release from Liposomes through Magnetic Actuation of Iron Oxide Nanoparticle Containing Membranes. *Nano Let.t* **2011**, *11*, 1664–1670.
26. Creixell, M.; Bohorquez, A. C.; Torres-Lugo, M.; Rinaldi, C. EGFR-Targeted Magnetic Nanoparticle Heaters Kill Cancer

Cells without a Perceptible Temperature Rise. *ACS Nano* **2011**, *5*, 7124–7129.
27. Rocha-Lima, C. M.; Soares, H. P.; Raez, L. E.; Singal, R. EGFR Targeting of Solid Tumors. *Cancer Control* **2007**, *14*, 295–304.
28. Roepstorff, K.; Grandal, M. V.; Henriksen, L.; Knudsen, S. L.; Lerdrup, M.; Grovdal, L.; Willumsen, B. M.; van Deurs, B. Differential Effects of EGFR Ligands on Endocytic Sorting of the Receptor. *Traffic* **2009**, *10*, 1115–1127.
29. Sorkin, A.; Goh, L. K. Endocytosis and Intracellular Trafficking Of ErbBs. *Exp. Cell Res.* **2008**, *314*, 3093–3106.
30. Latorre, M.; Rinaldi, C. Applications of Magnetic Nanoparticles in Medicine: Magnetic Fluid Hyperthermia. *P. R. Health Sci. J.* **2009**, *28*, 227–238.
31. Jordan, A. Hyperthermia Classic Commentary: `Inductive Heating of Ferrimagnetic Particles and Magnetic Fluids: Physical Evaluation of Their Potential for Hyperthermia' By Andreas Jordan *et al.*, *International Journal of Hyperthermia*, 1993;9:51−68. *Int. J. Hyperthermia* **2009**, *25*, 512–516.
32. Creixell, M.; Herrera, A. P.; Latorre-Esteves, M.; Ayala, V.; Torres-Lugo, M.; Rinaldi, C. The Effect of Grafting Method on the Colloidal Stability and *in Vitro* Cytotoxicity of Carboxymethyl Dextran Coated Magnetic Nanoparticles. *J. Mater. Chem.* **2010**, *20*, 8539–8547.
33. Kurz, T.; Gustafsson, B.; Brunk, U. T. Intralysosomal Iron Chelation Protects against Oxidative Stress-Induced Cellular Damage. *FEBS J.* **2006**, *273*, 3106–3117.
34. Lin, Y.; Epstein, D. L.; Liton, P. B. Intralysosomal Iron Induces Lysosomal Membrane Permeabilization and Cathepsin D-Mediated Cell Death in Trabecular Meshwork Cells Exposed to Oxidative Stress. *Invest. Ophthalmol. Visual Sci.* **2010**, *51*, 6483–6495.
35. Leist, M.; Jaattela, M. Triggering of Apoptosis by Cathepsins. *Cell Death Differ.* **2001**, *8*, 324–326.
36. Guicciardi, M. E.; Leist, M.; Gores, G. J. Lysosomes in Cell Death. *Oncogene* **2004**, *23*, 2881–2890.
37. Vertrees, R. A.; Zwischenberger, J. B.; Boor, P. J.; Pencil, S. D. Oncogenic RAS Results in Increased Cell Kill Due to Defective Thermoprotection in Lung Cancer Cells. *Ann. Thorac Surg.* **2000**, *69*, 1675–1680.
38. Hiramoto, Y.; Kusumoto, T.; Maehara, Y.; Sakaguchi, Y.; Kido, Y.; Ishida, T.; Sugimachi, K. Sarcoma-180 Cells Are More Sensitive to Heat than Are Mouse Normal Tissues: Esophagus, Stomach, Small Intestine, Large Intestine, Liver, Spleen, and Kidney. *J. Surg. Oncol.* **1989**, *40*, 170–172.
39. Tomasini, M. D.; Rinaldi, C.; Tomassone, M. S. Molecular Dynamics Simulations of Rupture in Lipid Bilayers. *Exp. Biol. Med.* **2010**, *235*, 181–188.
40. Huang, H.; Delikanli, S.; Zeng, H.; Ferkey, D. M.; Pralle, A. Remote Control of Ion Channels and Neurons through Magnetic-Field Heating of Nanoparticles. *Nat. Nanotechnol.* **2010**, *5*, 602–606.
41. Polo-Corrales, L.; Rinaldi, C. Monitoring Iron Oxide Nanoparticle Surface Temperature in an Alternating Magnetic Field Using Thermoresponsive Fluorescent Polymers. *J. Appl. Phys.* **2012**, *111*, 07B334.
42. Min, K. A.; Shin, M. C.; Yu, F.; Yang, M.; David, A. E.; Yang, V. C.; Rosania, G. R. Pulsed Magnetic Field Improves the Transport of Iron Oxide Nanoparticles through Cell Barriers. *ACS Nano* **2013**, *7*, 2161–2171.
43. Shen, J.-M.; Gao, F.-Y.; Yin, T.; Zhang, H.-X.; Ma, M.; Yang, Y.-J.; Yue, F. cRGD-Functionalized Polymeric Magnetic Nanoparticles as a Dual-Drug Delivery System for Safe Targeted Cancer Therapy. *Pharmacol. Res.* **2013**, *70*, 102–115.
44. Chertok, B.; David, A. E.; Yang, V. C. Brain Tumor Targeting of Magnetic Nanoparticles for Potential Drug Delivery: Effect of Administration Route and Magnetic Field Topography. *J. Controlled Release* **2011**, *155*, 393–399.
45. Li, S.; Schmitz, K. R.; Jeffrey, P. D.; Wiltzius, J. J.; Kussie, P.; Ferguson, K. M. Structural Basis for Inhibition of the Epidermal Growth Factor Receptor by Cetuximab. *Cancer Cell* **2005**, *7*, 301–311.
46. Trapp, S.; Rosania, G. R.; Horobin, R. W.; Kornhuber, J. Quantitative Modeling Of Selective Lysosomal Targeting For Drug Design. *Eur Biophys J* **2008**, *37*, 1317–1328.
47. Hallifax, D.; Houston, J. B. Saturable Uptake Of Lipophilic Amine Drugs into Isolated Hepatocytes: Mechanisms and Consequences for Quantitative Clearance Prediction. *Drug Metab. Dispos.* **2007**, *35*, 1325–1332.
48. Daniel, W. A.; Wojcikowski, J. Lysosomal Trapping as an Important Mechanism Involved in the Cellular Distribution of Perazine and in Pharmacokinetic Interaction with Antidepressants. *Eur. Neuropsychopharmacol.* **1999**, *9*, 483–491.
49. Chertok, B.; David, A. E.; Yang, V. C. Magnetically-Enabled and MR-Monitored Selective Brain Tumor Protein Delivery in Rats *via* Magnetic Nanocarriers. *Biomaterials* **2011**, *32*, 6245–6253.
50. Jordan, A.; Scholz, R.; Maier-Hauff, K.; Johannsen, M.; Wust, P.; Nadobny, J.; Schirra, H.; Schmidt, H.; Deger, S.; Loening, S. Presentation of a New Magnetic Field Therapy System for the Treatment of Human Solid Tumors with Magnetic Fluid Hyperthermia. *J. Magn. Magn. Mater.* **2001**, *225*, 118–126.
51. Creixell, M.; Herrera, A. P.; Ayala, V.; Latorre-Esteves, M.; Pérez-Torres, M.; Torres-Lugo, M.; Rinaldi, C. Preparation of Epidermal Growth Factor (EGF) Conjugated Iron Oxide Nanoparticles and Their Internalization into Colon Cancer Cells. *J. Magn. Magn. Mater.* **2010**, *322*, 2244–2250.